Nitrogen-enhanced greenhouse warming on early Earth

Colin Goldblatt[1,2]*, Mark W. Claire[3], Timothy M. Lenton[2], Adrian J. Matthews[2], Andrew J. Watson[2] and Kevin J. Zahnle[1]

Early in Earth's history, the Sun provided less energy to the Earth than it does today. However, the Earth was not permanently glaciated, an apparent contradiction known as the faint young Sun paradox. By implication, the Earth must have been warmed by a stronger greenhouse effect or a lower planetary albedo. Here we use a radiative–convective climate model to show that more N_2 in the atmosphere would have increased the warming effect of existing greenhouse gases by broadening their absorption lines. With the atmospheric CO_2 and CH_4 levels estimated for 2.5 billion years ago, a doubling of the present atmospheric nitrogen (PAN) level would cause a warming of 4.4 °C. Our new budget of Earth's geological nitrogen reservoirs indicates that there is a sufficient quantity of nitrogen in the crust (0.5 PAN) and mantle (>1.4 PAN) to have supported this, and that this nitrogen was previously in the atmosphere. In the mantle, N correlates with ^{40}Ar, the daughter product of ^{40}K, indicating that the source of mantle N is subducted crustal rocks in which NH_4^+ has been substituted for K^+. We thus conclude that a higher nitrogen level probably helped warm the early Earth, and suggest that the effects of N_2 should be considered in assessing the habitable zone for terrestrial planets.

Despite receiving less energy from the Sun in the Archaean and Proterozoic eras (for example, 83% of the present value at 2.5 billion years (Gyr) ago), the Earth was not subject to the permanent extreme glaciation that would have occurred if early Earth had its current albedo and greenhouse effect[1]. Most proposed solutions to the faint young Sun paradox focus on higher abundances of greenhouse gases (for example, CO_2, CH_4, NH_3, N_2O). Early work[1] favoured ammonia, but ammonia is soluble (so would have rained out) and is photochemically unstable[2]. Carbon dioxide is the obvious candidate[3], but palaeosol data constrain[4] pCO_2 to $(9.3 \times 10^{-3})^{\times 3}_{\div 3}$ bar (25 times the present atmospheric level) at 2.5 Gyr ago, which is insufficient by itself to prevent extreme glaciation. Methane[5] is a weak greenhouse gas in the palaeoclimate context and would need to be present at >1,000 ppm (>600 the present atmospheric level) to be effective[6]. N_2O may be important[7], but its palaeo-level is unknown. Water vapour is generally the strongest greenhouse gas, but its abundance is determined by temperature.

Alternatives are a lower planetary albedo (for example, if the early Earth was less cloudy) or a means of amplifying the greenhouse effect. Higher atmospheric pressure from N_2 would accomplish the latter; molecular absorption lines are widened by interactions with other molecules, a process known as pressure broadening or collision broadening. Pressure broadening moves absorption away from line centres, so more radiation is absorbed overall. In opposition to this, higher pressure increases the Rayleigh (molecular) scattering of incoming sunlight, thereby increasing planetary albedo. Comparative planetology provides inspiration: relative to planetary mass, Venus has 3.4 times as much nitrogen in its atmosphere as Earth. Atmospheres with 0.1 and 10 bar N_2 have been considered[8] in the context of the circumstellar habitable zone, but no calculations have been carried out for realistic early Earth values in the context of the faint young Sun. Here, we will show that (1) higher atmospheric pressure could have significantly warmed early Earth, (2) there is sufficient nitrogen in Earth's rocks to double or triple atmospheric pressure and (3) Earth's geological nitrogen probably originated in the atmosphere.

Nitrogen and climate

We investigate the effect of varying N_2 in a $H_2O–CO_2–CH_4$ greenhouse atmosphere using a radiative–convective climate model (RCM; see the Methods section) with a solar flux representative of 2.5 Gyr ago (see the Methods section). pN_2 is taken as 0.5, 1, 2 and 3 times the present level (0.79115 bar) and pCO_2 is varied between 1×10^{-4} and 2×10^{-2} bar (Fig. 1). Across the range of pCO_2, increasing pN_2 gives a strong increase in surface temperature, T_*, by 3–5 °C for pN_2 doubling and 5–8 °C for pN_2 tripling. Halving pN_2 decreases T_* by 3–5 °C. With $pCO_2 = 10^{-2}$ bar (26.5 times present level) at 2.5 Gyr ago, twice the present pN_2 would resolve the faint young Sun paradox, with $T_* = 11.8$ °C. Note that, although the threshold for runaway glaciation is taken as 6 °C in our model (see the Methods section), a genuine resolution to the faint young Sun paradox must be much warmer: a marginal resolution, near the threshold, would be characterized by extensive mid-latitude glaciation for which there is no evidence through most of the Archaean. $pCO_2 = 2 \times 10^{-2}$ bar under the present nitrogen inventory would give $T_* = 10.2$ °C (approaching a resolution) and double nitrogen would give $T_* = 15.0$ °C, a robust resolution.

To identify the radiative forcing from pressure broadening and Rayleigh scattering, we calculate fluxes in a set of fixed-temperature profiles (Fig. 2). We use a normalized pressure coordinate, $\sigma = p/p_*$, where p is pressure and p_* is surface pressure, so that the mass of radiative absorber in each layer in σ coordinates remains constant while pN_2 varies. To a first approximation,
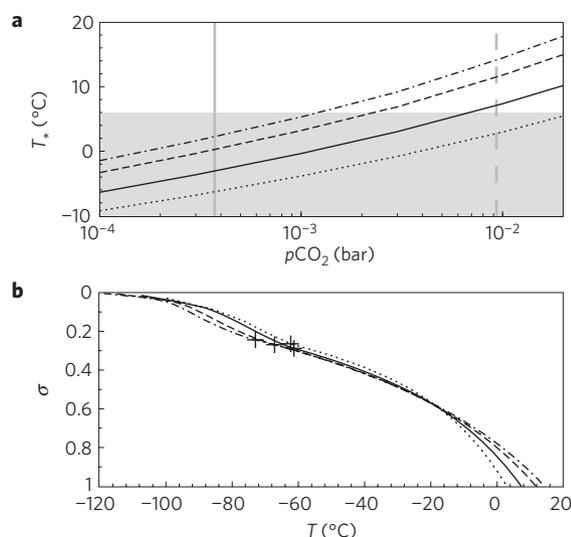
Figure 1 | Temperature change with increased nitrogen inventory from RCM runs. a, Surface temperature as a function of pCO_2. The vertical grey lines are present pCO_2 (solid) and 25 times present pCO_2 (dashed). Temperatures in the shaded area would lead to extreme glaciation (see the Methods section). **b**, Temperature profiles with 10^{-2} bar CO_2 ($\sigma = p/p_*$) and tropopause positions marked with crosses. The line styles (black lines) represent multiples of present N_2 inventory: dotted for 0.5, solid for 1, dashed for 2 and dashed–dotted for 3.

radiative absorption depends on the mass of absorber in a layer, so in the absence of pressure broadening the radiative fluxes for 0.5, 1, 2 and 3 times present pN_2 would be identical. However, the profiles of long-wave fluxes (Fig. 2b,d) show that increasing pressure gives strong radiative forcing (for example, $12.2 \, W \, m^{-2}$ at the tropopause for doubling pN_2, Fig. 2f), which will warm the planet. In the short-wave (Fig. 2a,c), increased Rayleigh scattering is dominant over increased absorption, giving a negative radiative forcing (for example, $-7.8 \, W \, m^{-2}$ at the tropopause for doubling pN_2, Fig. 2e), which partially counteracts warming.

A secondary process in warming the surface is a pressure feedback on the lapse rate, defined as $\Gamma = -dT/dz$, where T is temperature and z is altitude. We model this as the moist adiabatic lapse rate, in good agreement with global annual mean conditions[9]. Physically, convection occurs when the environmental lapse rate is greater than the moist adiabatic lapse rate. Convection decreases the environmental lapse rate until it equals the moist adiabatic lapse rate. The lapse rate of a pure radiative equilibrium atmosphere exceeds the moist adiabatic lapse rate, so the convective flux depends on the difference between these. The moist adiabatic lapse rate depends explicitly on pressure (see the Methods section; Fig. 3a). Increased pressure increases the moist adiabatic lapse rate, decreasing the amount of convection. This warms the surface (by up to 2 °C when N_2 is doubled (Fig. 3b)) and lower troposphere but cools the upper troposphere (Fig. 1b). There is also a surface temperature/lapse rate negative feedback; the moist adiabatic lapse rate decreases as temperature increases so there is more convection as surface temperature increases.

Generally, the positive water vapour feedback strongly affects temperature (water vapour is a potent greenhouse gas and the saturation vapour pressure, hence the mass of water vapour in the atmosphere, increases exponentially with temperature). Saturation vapour pressure is independent of atmospheric pressure, so changing nitrogen has no direct effect on this. However, water vapour feedback is induced indirectly through temperature changes arising from the radiative and dynamic forcings discussed above.

A new global nitrogen budget

Evidently, higher pN_2 can help resolve the faint young Sun paradox, but the following three questions are raised. (1) Where is the nitrogen now? (2) How did it get from the atmosphere to its present location? (3) When did this transfer take place?

There are three large and accessible nitrogen reservoirs on Earth: the atmosphere, crustal rocks and mantle. The PAN inventory is 4.0×10^{18} kg N (see the Methods section). The ocean and biosphere contain, respectively, two and three orders of magnitude less nitrogen than the atmosphere[10]. Quantifying geological nitrogen reservoirs is difficult owing to low concentrations, difficulties with atmospheric contamination and inaccessibility. In rock, nitrogen is generally present as NH_4^+ substituted for K^+ (refs 11, 12). Table 1 summarizes the planetary nitrogen budget developed here.

Nitrogen in crustal rocks

The classic and widely adopted estimates[13,14] use mass and nitrogen content of various rock types. More recent data allow us to revise these estimates. For the continental sediments, which have mass[15] 2×10^{21} kg and proportions[16] 40% shales (including clays and mudstones, 800 ppm N; refs 17, 12, 18, 19), 0% sandstones (200 ppm N; refs 12, 18) and 20% carbonates (100 ppm N; refs 12, 17), the total sedimentary nitrogen is 8.4×10^{17} kg N. For the remainder of the crust, which has mass[20] 1.9×10^{22} kg and proportions[14,21] 15% metasediments (250 ppm N, weighted towards mid and high grade)[11,22–24], 85% igneous and metamorphosed igneous rock (35 ppm N)[19], the total nitrogen is 1.3×10^{18} kg N. The total continental crust reservoir is then 2.1×10^{18} kg N.

Alternative estimates of sedimentary and metasedimentary reservoirs can be made with elemental ratios. N and K_2O concentrations in sediments are correlated[22], with $N/K_2O = 2.1 \times 10^{-2}$. 2.0 wt% K_2O in sediments[22] gives 420 ppm N; with sedimentary mass[15] 2×10^{21} kg, this gives a total of 8.4×10^{17} kg N. Using C/N, Holland[10] takes a crustal reduced carbon mass of 2×10^{19} kg C and a C/N weight ratio of 10, giving 2×10^{18} kg N. The C/N ratio of 10 is appropriate for recent oceanic sediments[17], but a C/N ratio of 20 is more appropriate for sedimentary rock and metasediments[23], which would give 1×10^{18} kg N.

Ocean crust is a smaller reservoir than continental crust. Sedimentary mass[15] is 7.4×10^{20} kg with nitrogen content[22] 420 ppm N, giving 3.1×10^{17} kg N. The basement consists of 0.5 km altered basalt (9 ppm N) and 6.5 km unaltered basalt (1.5 ppm N) (ref. 25), total 1.2×10^{16} kg N.

The main crustal reservoir is continental, and this contains ~0.5 PAN. Continental volume is usually thought to have increased from less than 10% of the present volume in the early Archaean to over 90% by the late Proterozoic[26]. The continental nitrogen inventory probably grew with continental volume. Nitrogen sequestration begins with biological nitrogen fixation and incorporation of nitrogen-rich organic matter into sediments. Although some nitrogen is lost during diagenesis, sedimentary rocks retain significant quantities[12,17–19]. Shelf sediments incorporate directly into continents. Deep-sea sediments can attach to continents as accretionary prisms. Nitrogen subducted in deep-sea sediments or in altered ocean crust (AOC) can be incorporated in igneous rocks in arc settings.

Nitrogen in the mantle

The large mass of the mantle (4.1×10^{24} kg) means that 1 PAN could be sequestered there at 1 ppm concentration. Nitrogen and argon measured in bubbles in mid-ocean-ridge basalt (MORB) and ocean island basalt (OIB) shows that N_2 correlates strongly with radiogenic ^{40}Ar but not primordial ^{36}Ar: $N_2/^{40}Ar \sim 80$ over several orders of magnitude in concentration, whereas $N_2/^{36}Ar$ varies by orders of magnitude[27,28]. ^{40}Ar is a daughter product of ^{40}K, so the correlation with N arises from substitution of
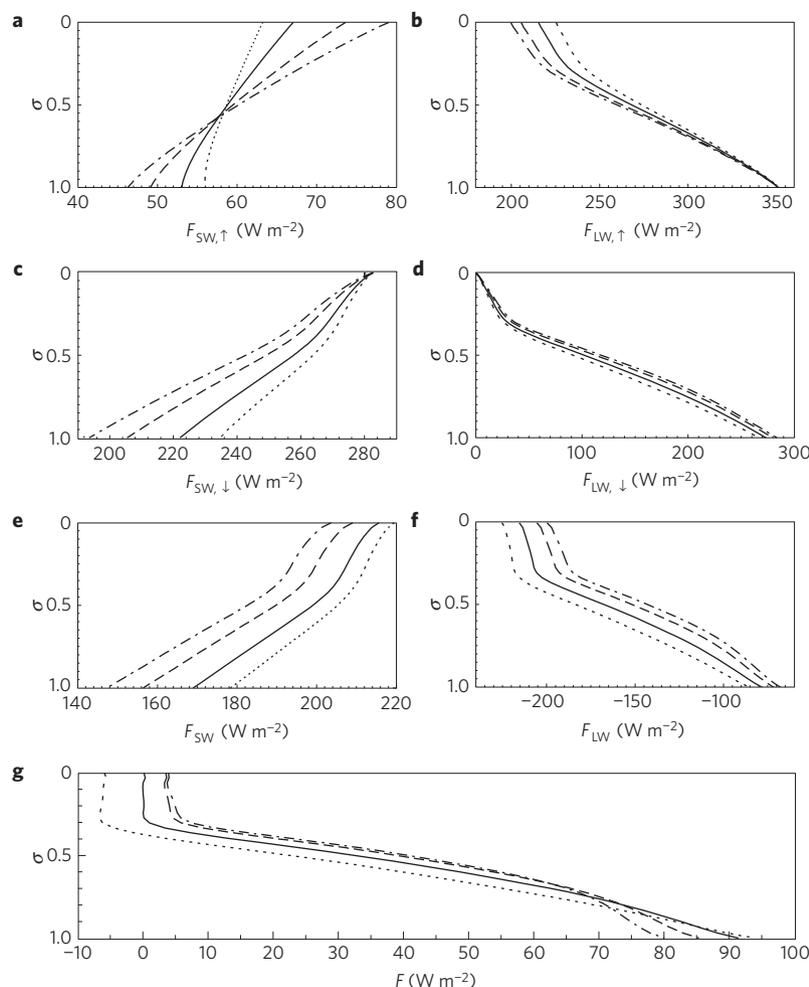
Figure 2 | Radiative effects of pressure broadening and Rayleigh scattering. A fixed profile of $T = T(\sigma)$, taken from the RCM run for present N_2 and 10^{-2} bar CO_2 is used (see Fig. 1b). Pressure is varied on this profile. **a,b**, Short-wave (**a**) and long-wave (**b**) upward fluxes. **c,d**, Short-wave (**c**) and long-wave (**d**) downward fluxes. **e,f**, Short-wave (**e**) and long-wave (**f**) net fluxes defined positive downwards, $F_j = F\downarrow_j - F\uparrow_j$ for each spectral region. **g**, Total flux $F = F_{LW} + F_{SW}$. The line styles represent multiples of present N_2 inventory: dotted for 0.5, solid for 1, dashed for 2 and dashed–dotted for 3.

NH_4^+ for K^+. The amount of ^{40}Ar produced through Earth history is $4.1 \pm 1.8 \times 10^{18}$ mol (see the Methods section). There are 1.7×10^{18} mol ^{40}Ar in the atmosphere, which implies that the remaining $2.4 \pm 1.8 \times 10^{18}$ mol ^{40}Ar are in the mantle. Assuming that nitrogen is incompatible with the solid phase of the mantle, so all nitrogen enters the melt, we calculate a lower bound for the nitrogen content of MORB and OIB source regions of the mantle: $N_2/^{40}Ar = 80 \pm 20$(ref. 28) gives $1.9 \pm 1.5 \times 10^{20}$ mol N_2 ($5.4 \pm 4.2 \times 10^{18}$ kg N), 1.4 times the present atmospheric nitrogen inventory. However, if nitrogen is partially compatible, then the mantle contains more nitrogen.

Two subreservoirs of the mantle may contain extra nitrogen, but are more difficult to assess. First, the subcontinental lithosphere contains subducted ocean crust material[29]. It is the main source region for diamond formation. Nitrogen concentrations in diamonds[30] are commonly up to 1,200 ppm. Estimates of mantle nitrogen content derived from diamonds[30] favour high concentrations, up to 40 ppm. Kimberlites often have a high N content[12], suggesting high N in their source in the upper mantle. As a tentative estimate, a concentration of 20 ppm N in 100 km of subcontinental lithosphere would give a reservoir ~3×10^{18} kg (0.75 PAN), although concentrations of between 2 and 40 ppm N are plausible. Second, the D'' layer at the core–mantle boundary might contain material from subducted slabs, so could contain a significant nitrogen inventory of atmospheric origin.

A key point is that the lack of correlation between N and primordial ^{36}Ar means that mantle N is not primordial and a history of monotonic volatile depletion of the mantle can be excluded. The strong correlation with radiogenic ^{40}Ar indicates that the main source of the mantle's nitrogen is NH_4^+ substituted for K^+. As K is incompatible and fractionates to crustal rocks, the mantle's N is from subducted crust.

Isotopic evidence also supports a subduction origin for mantle nitrogen[28]. When old cold slabs (dominant at present) are subducted they sink to the deep mantle, whereas when warm young slabs (more typical of the Archaean) subduct they remain in the upper mantle. The OIB source, which may sample the larger part of the mantle nitrogen inventory[28], has $\delta^{15}N = +3 \pm 2$ suggesting a source from deeply subducted, isotopically heavy, post-Archaean sediments. The MORB source material has $\delta^{15}N = -5 \pm 2$, suggesting that it samples isotopically light Archaean sediments[28,31], formed in the absence of oxygen, and subject to less deep subduction. Preservation of subducted sedimentary nitrogen also depends on the slab's characteristics: there is little change in nitrogen content of sedimentary and metasedimentary rocks subducting with old slabs[22,24,32], but with warmer slabs N loss[24] is ~75%.

We estimate the contemporary net nitrogen flux into the mantle as subduction input minus arc volcanic output. Subduction inputs consist of sediments[22] (7.6×10^8 kg N yr^{-1}), altered
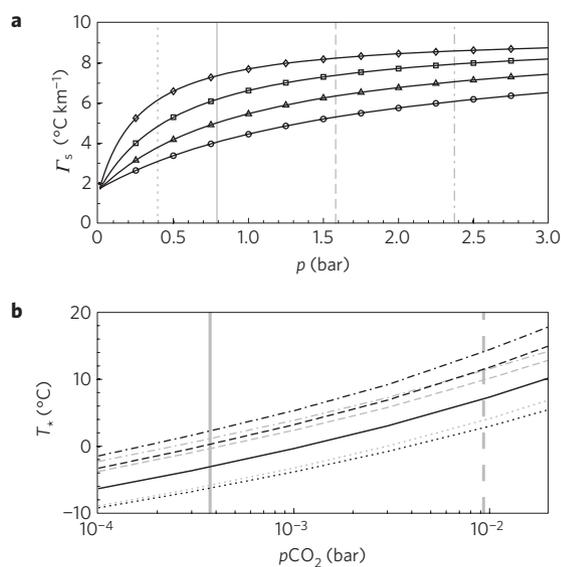
Figure 3 | Lapse rate feedback. a, Moist adiabatic (pseudoadiabatic) lapse rate with pressure and temperature. Markers represent temperatures of 260 K (diamonds), 270 K (squares), 280 K (triangles) and 290 K (circles). The vertical grey lines represent multiples of present N_2 inventory: dotted for 0.5, solid for 1, dashed for 2 and dashed–dotted for 3. **b**, Sensitivity experiment for lapse rate feedback on temperature. The RCM is run with varying nitrogen inventories, but with the lapse rate calculated from a fixed pressure profile, corresponding to present nitrogen inventory (grey lines), so no pressure/lapse rate feedback. Standard results with lapse rate feedback are shown in black for comparison. The line styles represent multiples of present N_2 inventory: dotted for 0.5, solid for 1, dashed for 2 and dashed–dotted for 3. The vertical grey lines are present pCO_2 (solid) and 25 times present pCO_2 (dashed).

Table 1 | Nitrogen budget.

Planet	Reservoir	Method	Nitrogen content (10^{18} kg N)
Venus	Atmosphere		10.8
	Atmosphere scaled to Earth mass		13.3
Earth	Atmosphere		4.0
	Continental crust		2.1 ± 1.1
	Igneous rock	Whole rock N	0.55 ± 0.27
	Metasediments	Whole rock N	0.71 ± 0.36
	Sedimentary rock	Whole rock N	0.84 ± 0.42
	(Sedimentary rock	N/K_2O	0.84 ± 0.42)
	(Sed. + Metased.	C/N	1.0 ± 0.5)
	Oceanic crust		0.32 ± 0.16
	Unaltered basalt	Whole rock N	$(3.9 \pm 2.0) \times 10^{-3}$
	Altered basalt	Whole rock N	$(8.5 \pm 4.2) \times 10^{-3}$
	Sediments	N/K_2O	0.31 ± 0.16
	Mantle		$\geq 8.4 \pm 5.2$
	MORB and OIB sources	K–Ar–N	5.4 ± 4.2
	Subcontinental lithosphere	Whole rock N	3 ± 3
	D'' layer	-	Unknown
	Total		14.8 ± 5.3

Estimated size of the large nitrogen reservoirs that can interact with the atmosphere over geological time. Atmospheric reservoirs are calculated with low uncertainty. For K–Ar–N systematics, uncertainty is propagated from original data. For other methods, an uncertainty of 50% is arbitrarily applied, except for the subcontinental lithosphere, which has 100% uncertainty. Alternative, supporting, estimates not used in totals are bracketed. Planetary cores may be very large nitrogen reservoirs as nitrogen is siderophilic, but are excluded here as core–mantle segregation occurred during Earth formation and they cannot interact with the atmosphere. For Earth, the core reservoir is estimated[50] as 9.75×10^{21} kg N.

oceanic crust (0.4×10^8 kg N yr^{-1}) and unaltered oceanic crust (0.8×10^8 kg N yr^{-1}), which total to 8.8×10^8 kg N yr^{-1}. The arc volcanic flux is estimated[33] as 5.5×10^8 kg N yr^{-1}. Thus, at present there is a significant net flux of subducted nitrogen to the mantle, 3.3×10^8 kg N yr^{-1}. The sign of this flux is confirmed by a detailed study across the Central American margin[17,25].

At the modern rate, only 0.4 PAN would have been transferred to the mantle since 4.5 Gyr ago. However, the ancient flux would have been higher when the deep ocean was anoxic and when tectonic cycling was faster. It is ammonium (NH_4^+) that incorporates into rock, but the NH_4^+ concentration in today's oxic deep ocean is negligible. Until[34] ~ 1.8 Gyr ago, the deep ocean was anoxic, so NH_4^+ would have been much more abundant (for example, anoxic Black Sea bottom waters contain[35] 40 μM NH_4^+). With abundant NH_4^+, much more nitrogen would incorporate into AOC (fluid inclusions in 3.2-Gyr-old hydrothermal basalts contain[36] ~ 10 mmol NH_4^+) and less sedimentary NH_4^+ would be lost in diagenesis, both increasing the nitrogen subduction flux. With higher geothermal heat flow and ocean spreading rate in the Archaean, more nitrogen would have been incorporated in AOC as this occurs during early hydrothermal activity[25]. Although AOC is a small (but perhaps preferentially preserved[25]) part of the nitrogen subduction budget at present, we envisage that it would have had a much larger role under both anoxic and fast spreading rate conditions.

When nitrogen transfer took place

Tentative inferences on when atmospheric nitrogen was drawn-down can be developed on the basis of major transitions in the Earth system: the origin of photosynthesis, deep-ocean oxidation and changing tectonic regime. Nitrogen fixation and sedimentary burial are biological, so will have increased concomitantly with productivity. Secular increases in productivity undoubtedly occurred with the origins of anoxygenic and oxygenic photosynthesis as productivity limitation changed from energetic to substrate to nutrient availability. Low productivity for much of the Archaean would give low nitrogen draw-down. Furthermore, nitrogen was probably outgassed from the mantle more rapidly then (high heat flow). Together, these would favour high atmospheric nitrogen. Extensive net removal of nitrogen was most likely for ~ 1 Gyr after the origin of oxygenic photosynthesis, but while the deep ocean remained anoxic. Thereafter, deep-ocean oxia may have throttled nitrogen burial and subduction.

Discussion

We review Earth's nitrogen budget, concluding that the total inventory is around three times the present atmospheric inventory. Mantle nitrogen is clearly subducted rather than primordial in origin. Continental nitrogen accumulated with continental volume. It is therefore likely that a higher fraction of Earth's nitrogen was previously in the atmosphere.

A high atmospheric nitrogen inventory in the Archaean would have geochemical consequences. First, hydrogen escape from Earth, the long-term cause of planetary oxidation, is diffusion limited so depends directly on the mixing ratio of total hydrogen in the upper atmosphere. For a given inventory of minor hydrogen-bearing species, doubling nitrogen would half the total hydrogen mixing ratio, the rate of hydrogen escape and planetary oxidation. Conversely, if methane-derived hydrogen escape balances a source of reductant from the solid Earth to maintain atmospheric redox balance[37], twice the pressure would imply twice the methane (so a stronger greenhouse) and the same oxidation rate. Second, as

it is reduced nitrogen (NH_4^+) that is sequestered in geological reservoirs, there is a net oxygen source (oxygenic photosynthesis followed by nitrogen fixation[11], net $N_2 + 3H_2O \rightarrow 2NH_3 + 1.5O_2$) to the extent that H is buried. Sequestration of 1 PAN as ammonium would liberate 2.1×10^{20} mol O_2, equivalent to 10% of the buried organic carbon[10] reservoir.

High nitrogen is not a single resolution to the faint young Sun paradox (we doubt that one exists), but higher nitrogen would translate an inventory of greenhouse gasses that was insufficient with the present nitrogen inventory into an effective resolution. In resolving the faint young Sun paradox, negative feedback cycles have a key role, especially the carbonate–silicate cycle. We have not identified such a cycle for nitrogen. Rather, nitrogen contributes a slowly changing (>100 million years) background on which changes in greenhouse gasses are superimposed. We have discussed the effect of pressure broadening by nitrogen for early Earth, but similar principles would apply for other terrestrial planets. For example, it might help explain the apparently warm and wet Noachian eon on Mars and would extend the 'habitable zone' for planets bearing liquid water.

Methods

Climate modelling. We use a radiative–convective model (RCM) to solve for the global annual mean vertical structure of the atmosphere. Convective adjustment in the model is to the pseudoadiabatic (moist) lapse rate. We assume a fixed relative humidity profile in normalized pressure coordinates[38] and a solar zenith angle of 60°. Radiative flux calculations use a narrowband (300 long-wave bands and 220 short-wave bands) radiance code[39]. The model uses a Newton–Raphson method to solve for equilibrium. The initial profile of temperature decreases linearly with pressure from 270 K at the surface to 230 K at the top of the atmosphere. The convergence threshold for radiative equilibrium is 0.2 W m^{-2}. Following the convention in RCMs used for palaeoclimate, we do not explicitly include clouds but use a high surface albedo to represent the net effect of clouds on the surface energy budget[40]. This simplifies the consideration of cloud feedbacks, which are highly uncertain, and facilitates direct comparison with other recent models[5,6]. For tuning runs, we represent the pre-industrial atmosphere with $pN_2 = 0.791$ bar, $pO_2 = 0.212$ bar, $pAr = 0.00942$ bar, $pCO_2 = 283 \times 10^{-6}$ bar, $pCH_4 = 0.709 \times 10^{-6}$ bar and a prescribed ozone profile[41]. We take the solar constant to be $S_0 = 1{,}368$ W m^{-2} and, to achieve a surface temperature of 288 K, we require a surface albedo of 0.24. For the palaeoclimate runs, we remove oxygen and ozone and enhance methane ($pCH_4 = 10^{-4}$ bar; ref. 37). We vary carbon dioxide in the range $10^{-4} < pCO_2 < 2 \times 10^{-2}$ bar and for N_2 use 0.5, 1, 2 and 3 PAN. The development and numerical method of the model has been described elsewhere[42]. The accuracy of the radiative transfer code used[39] in the RCM for calculating forcing from increased pCO_2 has been tested[43]: it is in good agreement with a line-by-line model[44] up to $pCO_2 \approx 10^{-2}$ bar but slightly underestimates forcings above that, affecting the highest pCO_2 included here. Testing the pressure broadening experiment against a line-by-line model[44] gives agreement within 0.5 W m^{-2} for the long-wave net flux at the tropopause when increasing N_2.

The runaway glaciation arises from the ice–albedo feedback. In models that explicitly represent this, the threshold for runaway glaciation is $\overline{T_*} \approx 0\,°C$. Similarly to other early Earth climate models[5,6,40], we do not attempt to represent the ice–albedo effect in our one-dimensional (vertical) radiative convective model. With the ice–albedo effect neglected, it is incorrect to use $\overline{T_*} \approx 0\,°C$ as the threshold for runaway glaciation. A model with the ice–albedo effect included would require a smaller drop in greenhouse-gas concentration than a model without this feedback. To account for this disparity, we first assume that the change in CO_2 to cause runaway glaciation in an ice-resolving model[45] is correct. We then apply the same CO_2 change to our model. The resulting model temperature, 6 °C, represents the effective threshold for runaway glaciation in our model.

Solar flux. In contrast to previous work[5,6,42], we derive a spectrally resolved solar flux for 2.5 Gyr ago, rather than multiplying the present spectrum by a constant. Solar models predict an effective temperature of 5,714.5 K at 2.5 Gyr ago[46]. We use ATLAS9 (ref. 47) with updated opacities[48] to compute a solar metallicity model atmosphere at 5,714.5 K, using standard values for stellar gravity ($\log g = 4.437$), microturbulence velocity (2 km s^{-1}) and pure mixing-length convection without overshooting ($L/H = 1.25$, where L/H is the ratio of mixing length to scale height)[48]. Microturbulence and L/H are not thought to be age dependent. Resulting stellar surface fluxes were normalized to 1 AU with an accounting for the smaller solar radii[46]. The smaller palaeo-radius results in a $\log g$ change of about 2%, which provides a negligible effect on the flux from the stellar surface, so we neglect this second-order effect. Using a spectrally resolved solar flux in place of a constant multiplier yields a planetary surface temperature 0.5 K higher.

Lapse rate feedbacks. The pseudoadiabatic (moist adiabatic) lapse rate is given by

$$\Gamma_s = \frac{g}{c_{pd}} \left(\frac{1 + \frac{L_{lv} w_s}{R_d T}}{1 + \frac{\varepsilon L_{lv}^2 w_s}{c_{pd} R_d T^2}} \right) \qquad (1)$$

where the saturation mixing ratio is

$$w_s = \varepsilon \frac{e_s}{p - e_s} \qquad (2)$$

and the saturation vapour pressure of water is

$$e_s = e_{s,tr} \exp\left[\frac{L_{lv}}{R_v} \left(\frac{1}{T_{tr}} - \frac{1}{T} \right) \right] \qquad (3)$$

where g is the acceleration owing to gravity, L_{lv} is the latent heat of vaporization of water, c_{pd} is the specific heat capacity of dry air, R_d and R_v are the gas constants for dry air and water vapour, p is pressure, $e_{s,tr}$ and T_{tr} are the saturation vapour pressure and temperature at the triple point and $\varepsilon = M_w/M_d$ is the ratio of molar masses of water vapour and dry air. Thus, pressure dependence in the lapse rate arises from equation (2) and temperature dependence from equations (1) and (3).

Atmosphere inventory. The atmospheric inventory can be calculated as

$$m_{N_2} = fN_2 \cdot \frac{M_{N_2}}{M_d} \cdot \frac{4\pi r_e^2 p_*}{g}$$

to give mass of N_2, $m_{N_2} = 3.98 \times 10^{18}$ kg, given mixing ratio $fN_2 = 0.7808$, molar masses of N_2 and dry air of $M_{N_2} = 28.01$ g mol^{-1} and $M_d = 28.97$ g mol^{-1}, acceleration owing to gravity $g = 9.81$ m s^{-2}, Earth radius $r_e = 6.371 \times 10^6$ m and $p_* = 101{,}325$ Pa.

K–N–Ar systematics. ^{40}K has half life $t_{1/2} = 1.248 \times 10^9$ yr, or decay constant $\lambda = 5.55 \times 10^{-10}$ yr^{-1}. 10.72% of this decay is by electron capture, producing ^{40}Ar, of which there is no other significant source. Thus, the inventory of ^{40}Ar is directly related to the amount of ^{40}K that has decayed and is calculated as: $[^{40}Ar]_0 = 0.1072(e^{(4.5 \times 10^{-9}\lambda)} - 1)[^{40}K]_0 = 1.20[^{40}K]_0$, where the subscript 0 is for present day. The natural abundance of isotope ^{40}K is 0.0117%, so $[^{40}K]_0 = 1.40 \times 10^{-4}[K]_0$. Taking the concentration of K in the silicate Earth (4.10×10^{24} kg) as 280 ± 120 ppm (ref. 49), the amount of ^{40}Ar produced through Earth history (the present inventory) is $4.11 \pm 1.76 \times 10^{18}$ mol ($1.64 \pm 0.70 \times 10^{17}$ kg). Uncertainties are stated as 2σ.

References

1. Sagan, C. & Mullen, G. Earth and Mars: Evolution of atmospheres and surface temperatures. *Science* **177,** 52–56 (1972).
2. Kuhn, W. R. & Atreya, S. K. Ammonia photolysis and the greenhouse effect in the primordial atmosphere of the Earth. *Icarus* **37,** 207–213 (1979).
3. Owen, T., Cess, R. D. & Ramanathan, V. Enhanced CO_2 greenhouse to compensate for reduced solar luminosity on early Earth. *Nature* **277,** 640–642 (1979).
4. Sheldon, N. D. Precambrian paleosols and atmospheric CO_2 levels. *Precambr. Res.* **147,** 148–155 (2006).
5. Pavlov, A. A., Kasting, J. F., Brown, L. L., Rages, K. A. & Freedman, R. Greenhouse warming by CH_4 in the atmosphere of early Earth. *J. Geophys. Res.* **105,** 11981–11990 (2000).
6. Haqq-Misra, J. D., Domagal-Goldman, S. D., Kasting, P. J. & Kasting, J. F. A revised, hazy methane greenhouse for the Archean Earth. *Astrobiology* **8,** 1127–1137 (2008).
7. Buick, R. Did the Proterozoic 'Canfield Ocean' cause a laughing gas greenhouse? *Geobiology* **5,** 97–100 (2007).
8. Kasting, J. F., Whitmere, D. P. & Reynolds, R. T. Habitable zones around main sequence stars. *Icarus* **101,** 108–128 (1993).
9. Ramanathan, V. & Coakley, J. A. Jr Climate modeling through radiative-convective models. *Rev. Geophys. Space Phys.* **16,** 465–489 (1978).
10. Holland, H. D. *The Chemistry of the Atmosphere and Oceans* (Wiley, 1978).
11. Boyd, S. R. Nitrogen in future biosphere studies. *Chem. Geol.* **176,** 1–30 (2001).
12. Holloway, J. M. & Dahlgren, R. A. Nitrogen in rock: Occurrences and biogeochemical implications. *Glob. Biogeochem. Cycles* **16,** 1118 (2002).

13. Wlotzka, F. in *Handbook of Geochemistry II* (ed. Wedepohl, K. H.) 7B1–7O3 (Springer, 1972).
14. Wedepohl, K. H. The composition of the continental crust. *Geochim. Cosmochim. Acta* **59,** 1217–1232 (1995).
15. Veizer, J. & Mackenzie, F. T. in *Treatise on Geochemistry* Vol. 7 (eds Holland, H. D. & Turekian, K. K.) 369–407 (Elsevier, 2003).
16. Amiotte Suchet, P., Probst, J.-L. & Ludwig, W. Worldwide distribution of continental rock lithology: Implications for the atmospheric/soil CO_2 uptake by continental weathering and alkalinity river transport to the oceans. *Glob. Biogeochem. Cycles* **17,** 1038 (2003).
17. Li, L. & Bebout, G. E. Carbon and nitrogen geochemistry of sediments in the Central American convergent margin: Insights regarding subduction input fluxes, diagenesis, and paleoproductivity. *J. Geophys. Res.* **110,** B11202 (2005).
18. Sullivan, P. J., Sposito, G., Strathouse, S. M. & Hansen, C. L. Geologic nitrogen and the occurrence of high nitrate soils in the western San Joaquin Valley, California. *Hilgardia* **47,** 15–49 (1979).
19. Hall, A. Ammonium in granites and its petrogenetic significance. *Earth. Sci. Rev.* **45,** 145–165 (1999).
20. Taylor, S. R. & McLennan, S. M. The geochemical evolution of the continental crust. *Rev. Geophys.* **33,** 241–265 (1995).
21. Rudnick, R. L. & Gao, S. in *Treatise on Geochemistry* Vol. 3 (eds Holland, H. D. & Turekian, K. K.) 1–64 (Elsevier, 2003).
22. Busigny, V., Cartigny, P., Philippot, P., Ader, M. & Javoy, M. Massive recycling of nitrogen and other fluid-mobile elements (K, Rb, Cs, H) in a cold slab environment: Evidence from HP to UHP oceanic metasediments of the Schistes Lustrs nappe (western Alps, Europe). *Earth Planet. Sci. Lett.* **215,** 27–42 (2003).
23. Mingram, B. & Bräuer, K. Ammonium concentration and nitrogen isotope composition in metasedimentary rocks from different tectonometamorphic units of the European Variscan Belt. *Geochim. Cosmochim. Acta* **65,** 273–287 (2001).
24. Bebout, G. E., Ryan, J. G., Leeman, W. P. & Bebout, A. E. Fractionation of trace elements by subduction-zone metamorphism—effect of convergent-margin thermal evolution. *Earth Planet. Sci. Lett.* **171,** 63–81 (1999).
25. Li, L., Bebout, G. E. & Idleman, B. D. Nitrogen concentration and $\delta^{15}N$ of altered oceanic crust obtained on ODP Legs 129 and 185: Insights into alteration-related nitrogen enrichment and the nitrogen subduction budget. *Geochim. Cosmochim. Acta* **71,** 2344–2360 (2007).
26. Hawkesworth, C. J. & Kemp, A. I. S. Evolution of the continental crust. *Nature* **443,** 811–817 (2006).
27. Tolstikhin, I. N. & Marty, B. The evolution of terrestrial volatiles: A view from helium, neon, argon and nitrogen isotope modelling. *Chem. Geol.* **147,** 27–52 (1998).
28. Marty, B. & Dauphas, N. The nitrogen record of crust–mantle interaction and mantle convection from Archean to Present. *Earth Planet. Sci. Lett.* **206,** 397–410 (2003).
29. Tappert, R. *et al.* Diamonds from Jagersfontein (South Africa): Messengers from the sublithospheric mantle. *Contrib. Mineral. Petrol.* **150,** 505–522 (2005).
30. Cartigny, P., Harris, J. W. & Javoy, M. Diamond genesis, mantle fractionations and mantle nitrogen content: A study of $\delta^{13}C$–N concentrations in diamonds. *Earth Planet. Sci. Lett.* **185,** 85–98 (2001).
31. Beaumont, V. & Robert, F. Nitrogen isotope ratios of kerogens in Precambrian cherts: A record of the evolution of atmosphere chemistry? *Precambr. Res.* **96,** 63–82 (1999).
32. Philippot, P., Busigny, V., Scambelluri, M. & Cartigny, P. Oxygen and nitrogen isotopes as tracers of fluid activities in serpentinites and metasediments during subduction. *Mineral. Petrol.* **91,** 11–24 (2007).
33. Hilton, D. R., Fischer, T. P. & Marry, B. Noble gases and volatile recycling at subduction zones. *Rev. Mineral. Geochem.* **47,** 319–370 (2002).
34. Canfield, D. E. A new model for Proterozoic ocean chemistry. *Nature* **396,** 450–453 (1998).
35. Konovalov, S. K., Murray, J. W., Luther, G. W. & Tebo, B. M. Processes controlling the redox budget for the oxic/anoxic water column of the Black Sea. *Deep-Sea Res. II* **53,** 1817–1841 (2006).
36. De Ronde, C. E. J., Channer, D. M. deR., Faure, C. J., Bray, K. & Spooner, E. T. C. Fluid chemistry of Archean seafloor hydrothermal vents: Implications for the composition of circa 3.2 Ga seawater. *Geochim. Cosmochim. Acta* **61,** 4025–4042 (1997).
37. Goldblatt, C., Lenton, T. M. & Watson, A. J. Bistability of atmospheric oxygen and the Great Oxidation. *Nature* **443,** 683–686 (2006).
38. Manabe, S. & Wetherald, R. D. Thermal equilibrium of the atmosphere with a given distribution of relative humidity. *J. Atmos. Sci.* **24,** 241–259 (1967).
39. Edwards, J. M. & Slingo, A. Studies with a flexible new radiation code. I: Choosing a configuration for a large scale model. *Q. J. R. Meteorol. Soc.* **122,** 689–719 (1996).
40. Kasting, J. F., Pollack, J. B. & Crisp, D. Effects of high CO_2 levels on surface temperature and atmospheric oxidation-state of the early Earth. *J. Atmos. Chem.* **1,** 403–428 (1984).
41. Jain, A. K., Briegleb, B. P., Minschwaner, K. & Wuebbles, D. J. Radiative forcings and global warming potentials of 39 greenhouse gases. *J. Geophys. Res.* **105,** 20773–20790 (2000).
42. Goldblatt, C. *Bistability of Atmospheric Oxygen, the Great Oxidation and Climate.* PhD thesis, Univ. East Anglia (2008).
43. Goldblatt, C., Lenton, T. M. & Watson, A. J. An evaluation of the longwave radiative transfer code used in the Met Office Unified Model. *Q. J. R. Meteorol. Soc.* **135,** 619–633 (2009).
44. Clough, S. A. *et al.* Atmospheric radiative transfer modeling: A summary of the AER codes. *J. Quant. Spectrosc. Ra.* **91,** 233–244 (2005).
45. Hyde, W. T., Crowley, T. J., Baum, S. K. & Peltier, W. R. Neoproterozoic 'snowball Earth' simulations with a coupled climate/ice-sheet model. *Nature* **405,** 425–429 (2000).
46. Bahcall, J. N., Pinsonneault, M. H. & Basu, S. Solar models: Current epoch and time dependences, neutrinos, and helioseismological properties. *Astrophys. J.* **555,** 990–1012 (2001).
47. Sbordone, L., Bonifacio, P., Castelli, F. & Kurucz, R. L. ATLAS and SYNTHE under Linux. *Mem. Soc. Astron. Ital. Supp.* **5,** 93 (2004).
48. Castelli, F. & Kurucz, R. L. in *Modelling of Stellar Atmospheres, IAU Symposium* Vol. 210 (eds Piskunov, N., Weiss, W. W. & Gray, D. F.) 20P (Astronomical Society of the Pacific, 2003).
49. Arevalo, Ricardo Jr, McDonough, W. F. & Luong, M. The K/U ratio of the silicate Earth: Insights into mantle composition, structure and thermal evolution. *Earth Planet. Sci. Lett.* **278,** 361–269 (2009).
50. Adler, J. F. & Williams, Q. A high-pressure X-ray diffraction study of iron nitrides: Implications for Earth's core. *J. Geophys. Res.* **110,** B01203 (2005).

Author contributions

C.G., T.M.L and A.J.W. suggested the study. C.G. wrote the RCM and carried out all model runs. C.G., A.J.M. and T.M.L. analysed the climate results. C.G. and K.J.Z. developed the nitrogen budget. M.W.C. calculated the changed solar flux.

Additional information